SP Science Press

ARTICLE

Recrystallization Mechanism of Typical Super-alloys

Shi Chenyi,   Zhang Maicang,   Guo Jing

School of Materials Science and Engineering, University of Science and Technology Beijing, Beijing 100083, China

Abstract: The dynamic and static recrystallization behavior of GH4760, GH4738, and AD730 typical Ni-based superalloys during hot deformation was investigated. The compressive hot deformation and solution annealing experiments were conducted. Results show that the nucleation mechanism of dynamic and static recrystallizations is dominated by the discontinuous mechanism of grain boundary bulging. Different types of stepped grain boundaries are generated during the dynamic and static recrystallizations due to the transformation from ordinary crystal planes into low-index crystal planes. This transformation results in lower energy of more grain boundaries. The morphology of the stepped boundaries on $\Sigma 3$ grain boundaries mostly decompose into $\{111\}_1/\{111\}_2$ and $90°\{112\}_1/\{112\}_2$ facets. The stepped grain boundaries promote the migration of grain boundaries, accelerating the recrystallization process. After recrystallization, partial stepped grain boundaries remain, the interfacial energy reduces, and the further grain growth is promoted.

Key words: Ni-based superalloys; stepped grain boundaries; nucleation mechanism of recrystallization

---

Ni-based superalloys strengthened by the γ' phase precipitation have high-temperature strength, hot corrosion resistance, and good oxidation resistance, and they have been widely applied in critical high-temperature components, such as aeroengine turbine disks and blades[1–3]. The excellent properties of Ni-based superalloys are determined by the alloy microstructure which is closely related to recovery and recrystallization. Recently, the recrystallization behavior of Ni-based superalloys has been extensively researched. Wang et al[4] evaluated the nucleation mechanism of dynamic recrystallization of GH4586 alloy at the strain of 20%−60% and the deformation temperature of 1273 and 1373 K. It is reported that the twinning can promote the growth of dynamic recrystallization grains, on the basis of the relationship between recrystallization fraction and twin boundary fraction. Liu et al[5] investigated the compression behavior of typical Ni-based superalloy at deformation temperature of 920−1040 °C and strain rate of $0.001 - 1$ s^{-1} and established a cellular automata model to accurately predict the size of dynamic recrystallized grains and the flow stress, which provided guidance for the prediction of dynamic recrystallization

behavior of Ni-based alloys.

Recrystallization usually involves the movement of grain boundaries and the defects accompanied with dislocations and step features. The serrated grain boundaries can be found in different alloys. Lee et al[6] investigated the relationship between grain boundary faceting and abnormal grain growth of polycrystalline Ni at different annealing temperatures, and revealed the relationship of the grain boundary structure with growth behavior. Generally, the grain boundaries with random misorientations undergo faceting transformation with changing the temperature and additives. Kim et al[7] found the serrated grain boundaries in AISI 316 stainless steel and studied the formation mechanism. The formation activation energy is consistent with the activation energy for carbon lattice diffusion in γ-iron, suggesting that the grain boundary serration can be controlled by the carbon lattice diffusion to grain boundaries. Hong et al[8] studied the formation mechanism of serrated grain boundary in wrought Ni-based Alloy-263 superalloy. It is found that the serrated grain boundary is triggered by the discontinuous segregation of C and Cr atoms at grain boundaries to release the excessive

---

elastic strain. Jiang et al[9] investigated the serrated grain boundary of solid solution-strengthened Haynes 230 alloy and found that the serrated grain boundary appears during slow cooling process, accompanied by the precipitation of intergranular $M_{23}C_6$ planar carbides, which have a coherent interface with the serrated grain boundary. The collective effect of the serrated grain boundaries and $M_{23}C_6$ carbides to reduce the interfacial energy and the unbalanced strain resulting from the discontinuous segregation of elements on the grain boundaries has been widely researched.

In this research, the recrystallization behavior during hot deformation and the subsequent solid solution treatment of different superalloys were investigated. The selected Ni-based superalloys were the ultra-supercritical power station hot-end component alloy (GH4760), the high-quality alloy used for aeroengine (GH4738), and AD730 alloy. GH4760 alloy is a novel nickel-based superalloy based on the optimal design of composition and microstructure of Inconel740H alloy (High Temperature Materials Laboratory of University of Science and Technology Beijing). GH4738 alloy is a γ' precipitation-strengthened nickel-based wrought superalloy (Waspaloy)[10]. A forged square bar of AD730 alloy (Aubert & Duval Co., Ltd) was used in this research[2].

The generation mechanism of stepped grain boundaries and their impact on grain boundary migration during the dynamic and static recrystallization of alloys were analyzed. This research provided a theoretical basis for the investigation of the relationship between the grain boundary structure and the grain boundary migration during hot deformation.

1 Experiment

The chemical composition of the GH4760, GH4738, and AD730 alloys is listed in Table 1. GH4738 and AD730 alloys were obtained from the forged bars, and the GH4760 alloy was obtained from the forged bar and the cold-rolled pipe. Cylindrical specimens with 10 mm in diameter and 15 mm in height were cut axially from the forged bars and cold rolled billets. Then the specimens were compressed by MTS810-25T low-cycle fatigue tester to analyze the nucleation mechanism of dynamic recrystallization. The hot deformation process is shown in Fig. 1. The deformation temperatures for GH4760 alloy were 1000, 1050, 1100, 1150, and 1200 °C; those for GH4738 alloy were 1020, 1040, 1060, 1080, and 1100 °C; those for AD730 alloy were 1040, 1080, 1100, 1120, and 1140 °C. The strain rates for GH4760 alloy were 0.01, 1, 10, and 20 s^{-1}; those for GH4738 alloy were 0.01, 0.1, and 1 s^{-1}; those for AD730 alloy were 0.01, 1, and 5 s^{-1}. The strain was 50%. All specimens were heated to the deformation temperatures at heating rate of 10 °C/s and held for about 3

min to ensure the temperature uniformity before deformation. After the compression tests, the specimens were water-quenched for microstructure observation. Afterwards, the specimens were cut along the compression axis and then mechanically ground and polished. Then the specimens were boiled in 2.5 g $KMnO_4$+10 mL H_2SO_4+90 mL H_2O solution for 5 min, washed, and dried. The grain structure was observed by DMR optical microscope (OM). The foils of 0.3 mm in thickness for transmission electron microscope (TEM) observation were cut from the specimens, mechanically ground to 50 μm in thickness, and subsequently punched to disks with diameter of 3 mm. The disks were thinned by twin-jet electropolishing with solution of 5vol% perchloric acid in ethanol. Microstructure analysis was conducted by JEM-2010 TEM. Grain boundary structure at nanoscale was studied through the high resolution TEM (HRTEM). The longitudinal section of the specimen was observed by OM and TEM.

The cold-rolled GH4760 specimens (10 mm×10 mm×5 mm) were solution-annealed at 1100, 1120, 1140, 1160, and 1180 °C, and the hot-deformed GH4738 specimens were solution-annealed at 1020, 1040, 1060, and 1080 °C to evaluate the nucleation mechanism of static recrystallization. The GH4760 specimens were held at solution annealing temperatures for 10, 20, and 40 min, and GH4738 specimens were held for 5, 10, and 20 min. The specimens after solid solution were observed through OM and TEM, and the static recrystallization behavior was analyzed.

2 Results and Discussion

2.1 Microstructure and nucleation mechanism of dynamic recrystallization during hot deformation

The microstructure of longitudinal section of the forged specimens of GH4760 alloy is shown in Fig. 2. The original microstructure of the forged specimens is not uniform, and several non-recrystallized zones can be observed. Fig. 3 displays several recrystallized microstructures of GH4760 alloys after hot deformation under different conditions. The alloy recrystallization occurs after compressive deformation under different conditions. The original forged microstructure is transformed into the uniform dynamic recrystallization microstructure. In addition, the lower the strain rate, the more complete the recrystallization process. The effect of strain rate on grain size is slight. The grain size is increased obviously with increasing the deformation temperature. Furthermore, the dynamic recrystallization grains after deformation at strain rate of 0.01 s^{-1} exhibit the grain boundary bowing phenomenon, i.e., the bulging grain boundary occurs.

Fig. 4 shows TEM morphologies of different Ni-based

Table 1   Chemical composition of GH4760, GH4738, and AD730 superalloys (wt%)

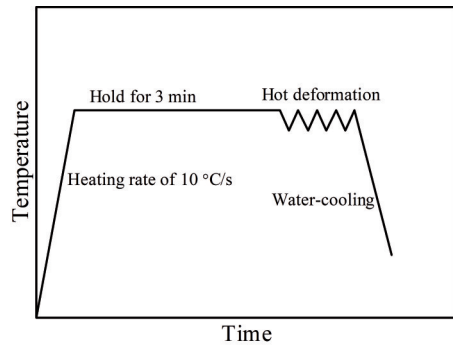| Alloy	Cr	Co	Mo	Al	Ti	W	Fe	Nb	Zr	C	B	Ni
GH4760	24.5	12.0	0.5	1.3	1.6	-	-	1.3	-	0.03	-	Bal.
GH4738	19.14	13.34	4.42	1.46	3.24	-	-	-	-	0.029	0.0042	Bal.
AD730	15.7	8.5	3.1	2.25	3.4	2.7	4.0	1.1	0.03	0.015	0.01	Bal.

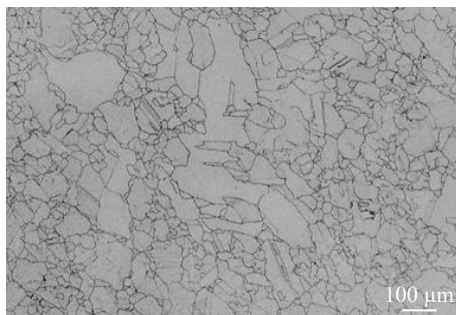Fig.1   Schematic diagram of hot deformation process

Fig.2   Microstructure of longitudinal section of forged GH4760 alloy bar

superalloys under different hot deformation conditions. As shown in Fig. 4, the grain boundary bowing phenomenon can be observed in all alloys under different compressive deformation conditions, indicating that the dynamic recrystallization mainly occurs through the discontinuous nucleation. According to Fig.4b, the bulging grain boundary is cut off by twins, which may promote the process of recrystallization. Li et al[11] investigated the microstructure evolution of dynamic recrystallization of Inconel 718 alloy, and found that the original grain boundaries can be transformed into different twins to accelerate the dynamic recrystallization. Cao et al[12] explored the nucleation mechanism of dynamic recrystallization and the effect of twins on dynamic recrystallization of Ni-Cr alloy (800H). It is revealed that the twinning has significant influence on the reduction of grain boundary energy: the twinning can accelerate the grain boundary mobility and contribute to the recrystallization process.

Ni-based alloys have low-stacking-fault energy, so the cross slip and climbing of dislocations during hot deformation can hardly proceed. The recovery process is hindered, and the dynamic recrystallization predominantly occurs. The polycrystalline deformation is non-uniform, and therefore the grains with different orientations are subject to different strains. The grains with large strains have high dislocation densities, whereas those with small strains have low dislocation densities. As a result, the significant dislocation density difference between the two sides of grain boundaries can be observed during deformation. These differences cause the original grain boundary to bend from the low-dislocation-density side to the high-dislocation-density side until a certain shape with stable interface is obtained. The bulging grain boundaries are shown in Fig. 4. According to the classical theory of strain-induced grain boundary migration (SIBM)[13], the dislocation densities in the grains on two sides of the grain boundary are different, and the actual core can only be formed by satisfying the relationship, as expressed by Eq. (1), as follows:

$$\Delta E \geq 2\varepsilon_b / L \tag{1}$$

where ΔE is the difference in storage energy per unit volume on both sides of the bulging grain boundary, ε_b is the grain boundary energy, and L is the half length of original grain boundary related to the bulging grain boundary.

Under the low strain rate condition, the deformation duration is long, and the discontinuous dynamic
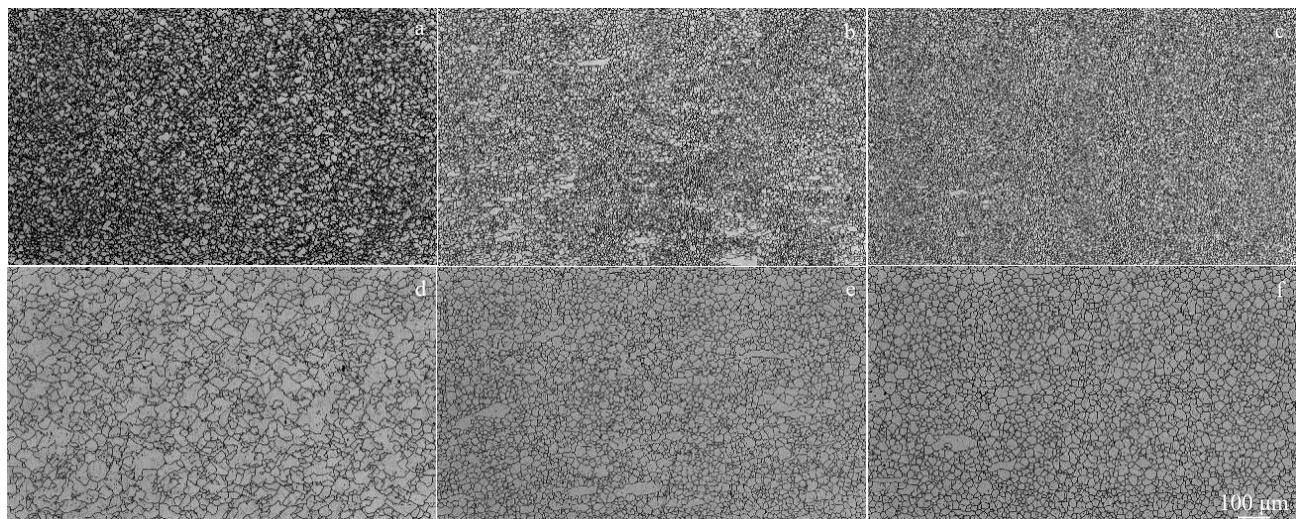

Fig.3   Microstructures of GH4760 alloys after hot deformation under different conditions: (a) 1050 °C/0.01 s^{-1}; (b) 1050 °C/10 s^{-1}; (c) 1050 °C/20 s^{-1}; (d) 1150 °C/0.01 s^{-1}; (e) 1150 °C/10 s^{-1}; (f) 1150 °C/20 s^{-1}
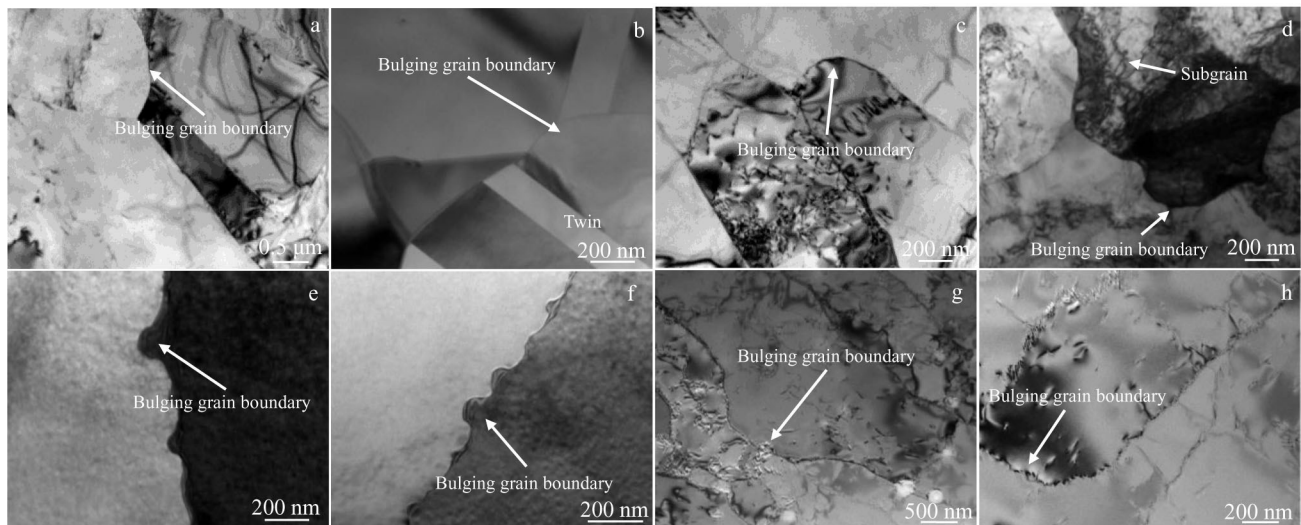
Fig.4   TEM morphologies of Ni-based alloys under different hot deformation conditions: (a) GH4760/1050 °C/0.01 s^{-1}; (b) GH4760/1150 °C/ 0.01 s^{-1}; (c) GH4760/1050 °C/20 s^{-1}; (d) GH4760/1150 °C/20 s^{-1}; (e) AD730/1120 °C/1 s^{-1}; (f) AD730/1100 °C/5 s^{-1}; (g) GH4738/1040 °C/ 0.01 s^{-1}; (h) GH4738/1060 °C/0.01 s^{-1}

recrystallization dominated by the bulging grain boundary proceeds completely. Recrystallized grains have sufficient time to grow, and the grain boundary bowing phenomenon occurs again, resulting in a new cycle of discontinuous dynamic recrystallization. OM and TEM analysis results show that the main recrystallization nucleation mechanism at low strain rate is discontinuous bulging. The deformation duration is decreased with increasing the strain rate. Thus, the regional dislocations cannot be eliminated, and the duration of dynamic recrystallization is restricted. The grain growth of dynamic recrystallization is inhibited at high strain rate, and the scattered dislocations still exist in the grains, as shown in Fig.4c and 4d.

When the strain rate is constant and the deformation temperature is low, the cross slip of screw dislocations and the climbing of edge dislocations are weak. The Ni-based alloys deformed at low temperatures have high dislocation densities, as indicated by Fig. 4a and 4c. The atomic thermal activation capability is enhanced with increasing the deformation temperature, and several potential slip systems are activated, forming a small number of sub-grain boundaries which are favorable for recrystallization nucleation, as shown in Fig.4d. In addition, the increased deformation temperature can enhance the migration capability of the recrystallized grain boundary and accelerate the dislocation annihilation, thereby reducing the dislocation density of the alloys. After deformation at high temperatures, the low dislocation density, clear and sharp grain boundary, and a large dynamic recrystallized grain size can be obtained for the Ni-based alloys.

2.2 Microstructure and nucleation mechanism of static recrystallization after solution annealing

Fig. 5 shows the microstructure of the longitudinal section of cold-rolled GH4760 alloy pipe before solid solution. The
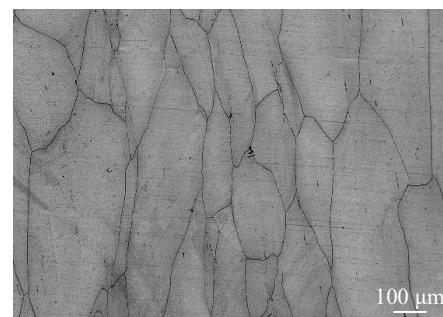

Fig.5   Microstructure of longitudinal section of cold-rolled GH4760 alloy pipe

grains are elongated parallel to the rolling direction, presenting the cold deformation characteristics. Fig.6 presents the microstructures of GH4760 alloys after different solid solution treatments. When the solid solution temperature is 1100 °C, a large number of fine equiaxed grains appear, but the microstructure is still non-uniform. The grains are gradually increased and become uniform with increasing the solid solution temperature. In addition, the grains are gradually increased with prolonging the solution duration. Notably, the recrystallization is completed in a short period during the solid solution at 1180 °C. With further prolonging the treatment duration, the grains mainly grow.

Fig. 7 shows TEM morphologies of cold-rolled and solid-solution-treated GH4760 alloys. A large number of dislocation nets and deformation slabs can be observed in the cold-rolled GH4760 alloy. With increasing the solid solution temperature or prolonging the solid solution duration, the recrystallization is accelerated, and the dislocation density is gradually reduced. The dislocation density difference can be found on both sides of large-angle grain boundaries.

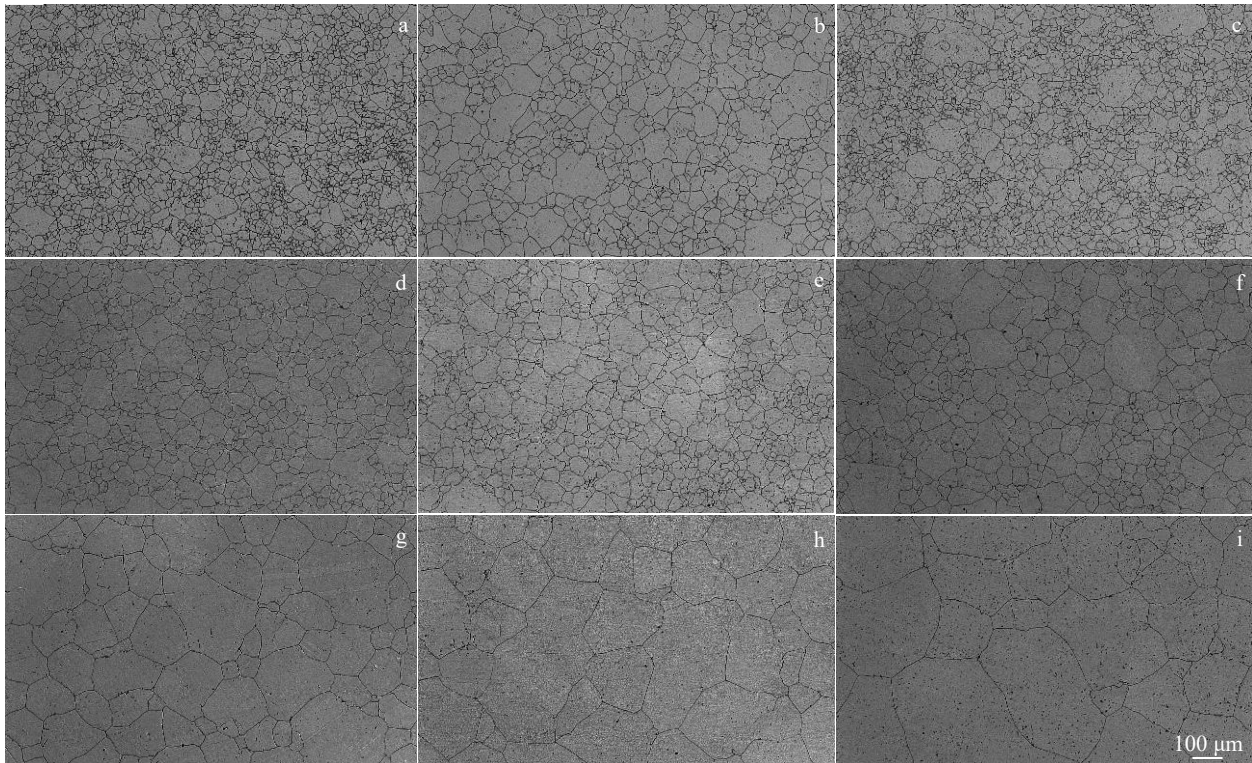The driving force for static recrystallization is the

Fig.6   Microstructures of GH4760 alloys after different solid solution treatments: (a) 1100 °C/10 min; (b) 1100 °C/20 min; (c) 1100 °C/40 min; (d) 1140 °C/10 min; (e) 1140 °C/20 min; (f) 1140 °C/40 min; (g) 1180 °C/10 min; (h) 1180 °C/20 min; (i) 1180 °C/40 min
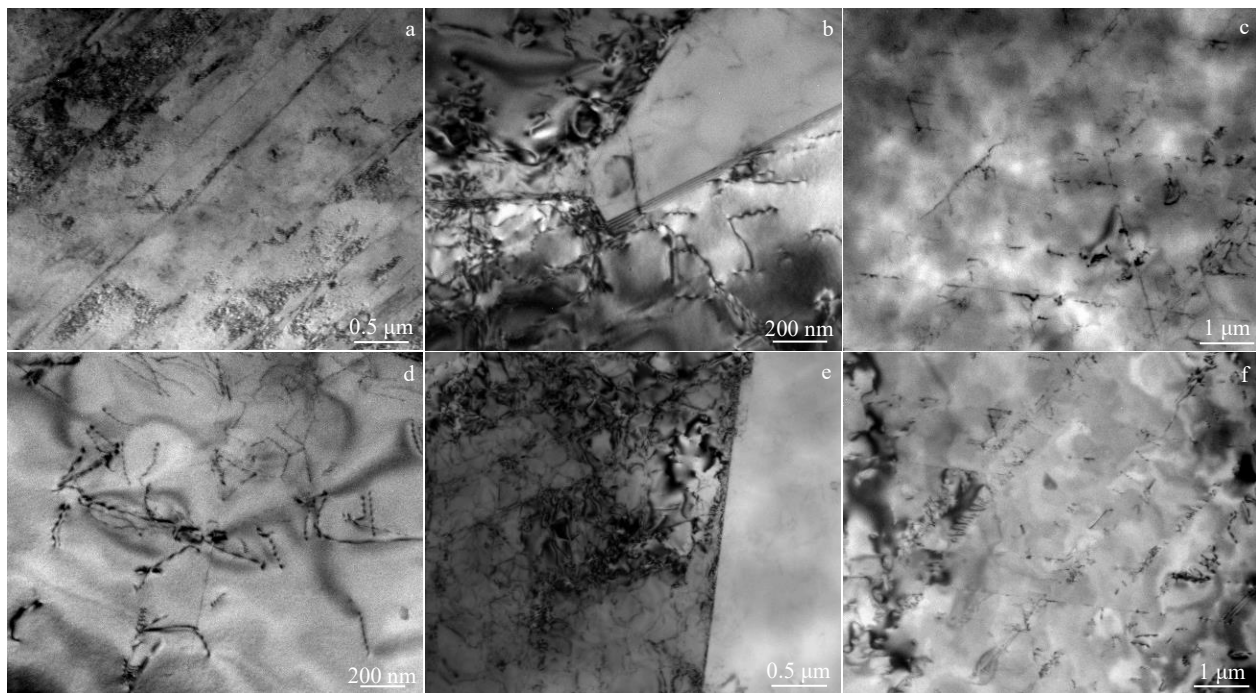

Fig.7   TEM morphologies of dislocation evolution in cold-rolled (a) and solid-solution-treated (b−f) GH4760 alloys under different conditions: (b) 1100 °C/20 min; (c) 1140 °C/20 min; (d) 1180 °C/20 min; (e) 1140 °C/10 min; (f) 1140 °C/40 min

mechanical storage energy of deformed alloys, which satisfies the thermal condition of recovery and recrystallization. The rate of static recrystallization is increased with increasing the annealing temperature. Therefore, increasing the annealing temperature and prolonging the annealing duration are beneficial to the grain growth, microstructure uniformity, and the release of deformation storage energy in alloys. Similarly, the static recrystallization results from the difference in

dislocation density between the original large-angle grain boundaries caused by deformation, and the main recrystallization nucleation mechanism is SIBM nucleation.

2.3 Mechanism of stepped grain boundaries during recrystallization

Fig. 8 shows the stepped grain boundaries generated in different Ni-based alloys during dynamic recrystallization. As shown in Fig. 8a, an approximately right-angled stepped sharp grain boundary can be observed. The width of stepped grain boundary platform is $0.2-0.5$ μm. According to Fig. 8b, the grain boundaries are transformed into the faceted hill-and-valley structure at some sites, which is similar to the grain boundary morphology in pure nickel during abnormal grain growth[6]. The edges of the stepped grain boundaries are no longer straight lines, and the corner appears to be round, as shown in Fig. 8c. The stepped grain boundary morphology in Fig. 8d is similar to that in Fig. 8a, except for the difference in width and height. The stepped grain boundary can be found in alloys under various solid solution conditions, and the right-angled stepped grain boundaries are common. However, the number of stepped grain boundaries at high temperatures is small, and the transition occurs in the grain boundary with the finite length.

Fig. 9 shows the stepped grain boundaries in different Ni-based alloys during static recrystallization. The stepped grain boundaries in Fig. 9a – 9c are similar to those in Fig. 8, presenting almost straight steps. Fig.9d shows that the stepped grain boundary appears at the annealing twin boundary[14]. All edges between the facets are sharp and various facets exist concurrently. Their crystallography relationship is consistent with the facets at Σ3 grain boundaries in copper[15–16].

Fig. 10 shows the stepped grain boundaries and corresponding selected area electron diffraction (SAED) patterns during static recrystallization of GH4738 alloys. The right-angled steps can be observed in GH4738 alloys after different solid solution treatments. According to Fig. 10c, the stepped grain boundary is twin boundary with $\Sigma=3$ coincidence site lattice (CSL). According to Fig. 10d, the superposition of two sets of ordinary diffraction patterns instead of the diffraction peaks of twin boundary is observed. It should be noted that the superimposed SAED pattern is similar to SAED pattern of the grain with $[\bar{1}11]$ axis because of the large misorientation between adjacent grains, and the complete SAED pattern of the grains with $[\bar{1}14]$ axis can only be obtained after tilting to a certain angle. After further analysis, it can be proved that one side of the stepped grain boundary is twin boundary and the other is the grain boundary with other orientations.

The straight steps on Σ3 grain boundary are formed during the static recrystallization of GH4738 alloy, as shown in Fig. 11. Fig. 11a shows the stepped grain boundaries along the [110] zone axis (DB), and the edges of twin boundaries are sharp. A series of steps with different widths and heights can be clearly observed, and the angles between them are approximately 90° . Fig. 11b shows HRTEM image of horizontal stepped grain boundary obtained along the [110] zone axis corresponding to the rectangular area in Fig. 11a, which is the most closely packed CSL plane $(\bar{1}11)_M/(\bar{1}11)_T$ (the subscripts T and M represent the twin and matrix, respectively). Fig. 11c displays the fast Fourier transform (FFT)
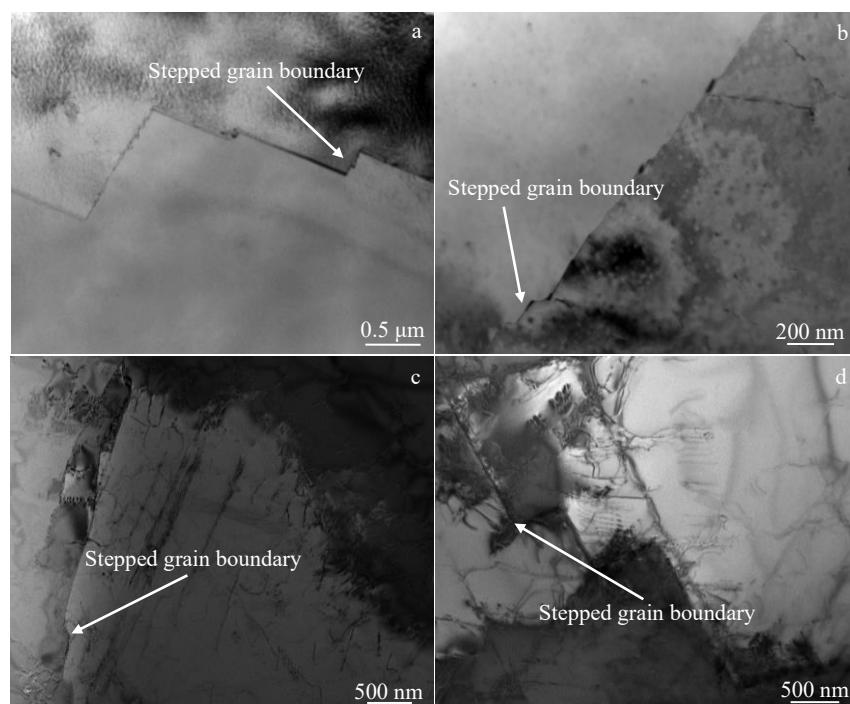

Fig.8   Stepped grain boundaries in different Ni-based alloys during dynamic recrystallization under different conditions: (a) AD730/1100 °C/ 5 s^{-1}; (b) AD730/1120 °C/1 s^{-1}; (c) GH4738/1060 °C/0.01 s^{-1}; (d) GH4738/1080 °C/0.01 s^{-1}
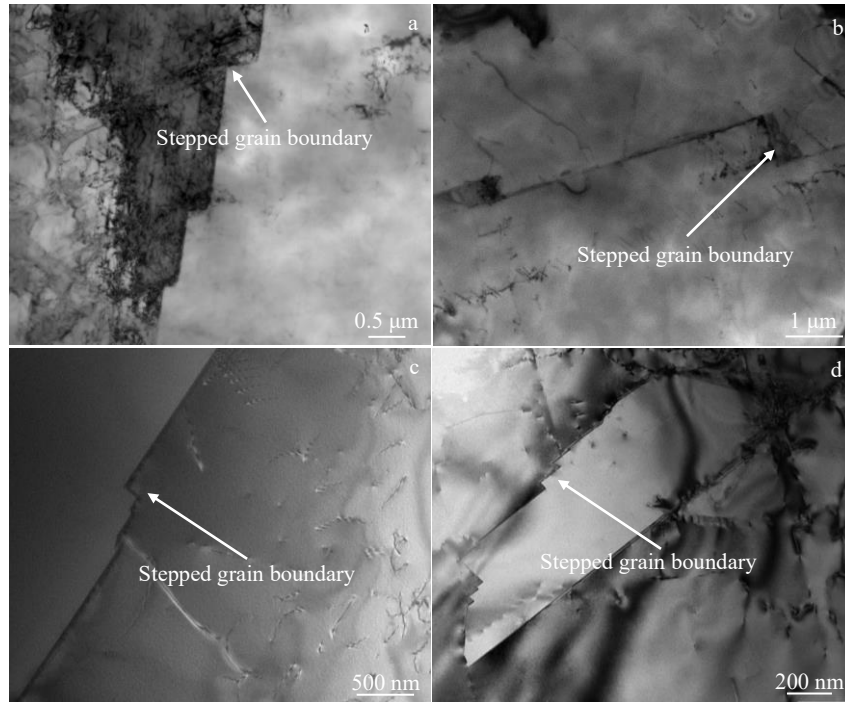
Fig.9 Stepped grain boundaries in different Ni-based alloys during static recrystallization under different conditions: (a) GH4760/1140 °C/ 10 min; (b) GH4760/1140 °C/20 min; (c) GH4738/1040 °C/5 min; (d) GH4738/1040 °C/10 min
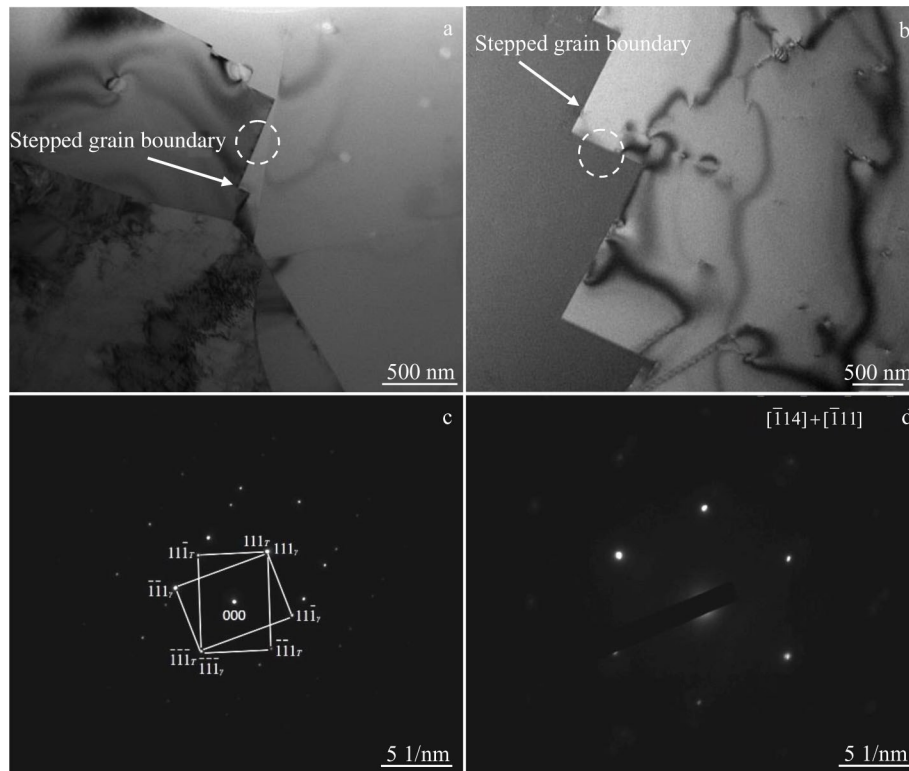

Fig.10 TEM morphologies of stepped grain boundaries in GH4738 alloys after solid solution treatments of 1040 °C/5 min (a) and 1060 °C/ 5 min (b); SAED patterns corresponding to circle areas in Fig.10a (c) and Fig.10b (d)

image of the Σ3 twin boundary plane with inclination angle of 39° around the [110] axis, which is a coherent Σ3 $\{111\}_1/\{111\}_2$ symmetric grain boundary. Fig.11e shows the vertical section of stepped grain boundary in the rectangular area in Fig.11a, which is the less closely packed CSL plane $(1\bar{1}2)_T/(1\bar{1}2)_M$ with incoherent Σ3 $\{112\}_1/\{112\}_2$ grain boundary. According to
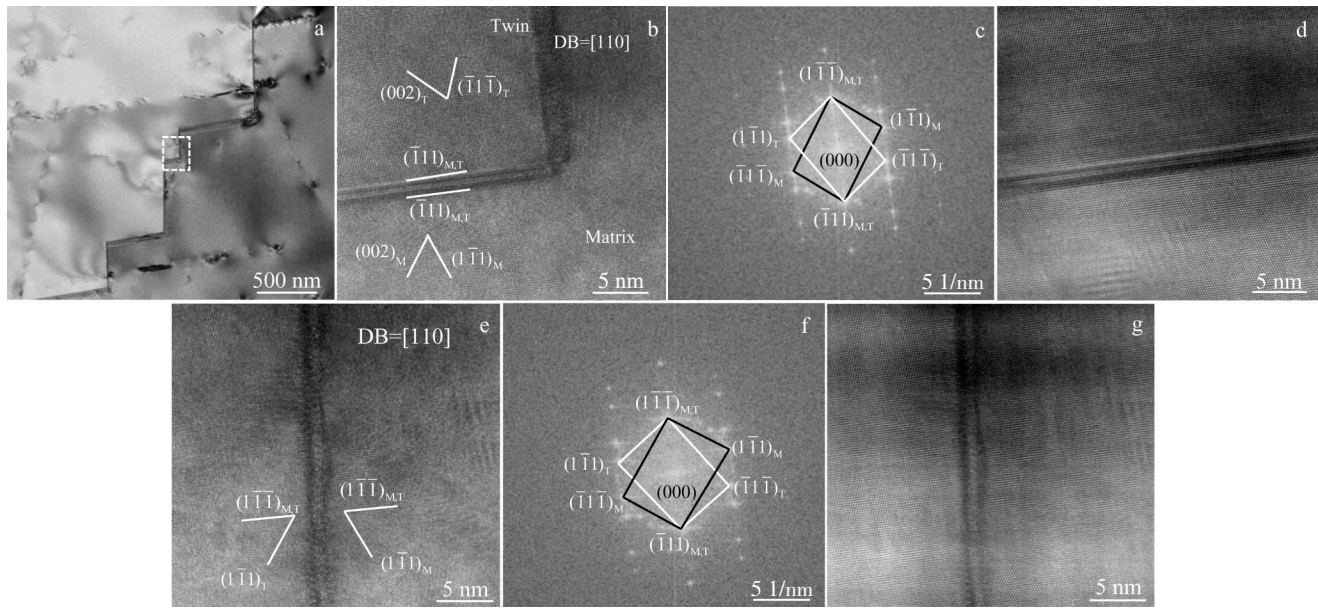
Fig.11   TEM morphology of straight steps on Σ3 grain boundary during static recrystallization of GH4738 alloy (a); HRTEM images of horizontal (b) and vertical (e) sections of stepped grain boundaries in rectangular area of Fig. 11a; FFT images (c, f) and ABSF-filtered images (d, g) corresponding to Fig. 11b (c, d) and Fig. 11e (f, g)

Fig. 11f, the inclination angle between twin boundary planes is 38.99°. The straight stepped grain boundary is similar to a special facet structure which consists of Σ3 $\{111\}_1/\{111\}_2$ coherent twin boundary and incoherent Σ3 $\{112\}_1/\{112\}_2$ twin boundary. According to the junction of the crystal faces, it is not a symmetrical plane, but still a sharp edge. Fig. 11d and 11g are the average background subtraction filter (ABSF)-filtered images of Fig. 11b and 11e, respectively. Fig. 11d shows the coherent twin boundary, where atoms are tightly packed, presenting a sharp interface. However, the atoms are less-closely packed, as shown in Fig. 11g, presenting the coarse crystal interface. All the straight stepped grain boundaries are similar, so the ones in Fig. 11a are composed of Σ3 $\{111\}_T/\{111\}_M$ and $\{112\}_T/\{112\}_M$.

The principle of grain boundary faceting is the same as the thermodynamic principle of crystal surface. The surface energy of the crystal depends on the surface orientation, and its equilibrium shape can be obtained by Wulff diagram when the volume remains constant. A crystal-free surface has an intact low-energy surface (low-index plane) in the equilibrium state. However, the crystal surface will deviate from the low-energy surface in the actual non-equilibrium hot deformation. The vicinal surface with slight offset from the low-energy surface usually occupies most of the surface, and then the vicinal surface is faceted. Therefore, several atoms are transferred from the original position to other positions to form a new oriented facet (Fig. 12), which reduces the surface energy. The surface contains platform, step, and kink: the platform is the low-index closely-packed plane with low energy; the steps and kinks are formed to ameliorate the deviation of the surface to ensure that more surfaces have low energy. In Fig. 12, θ is the deviation angle, h is the step height,
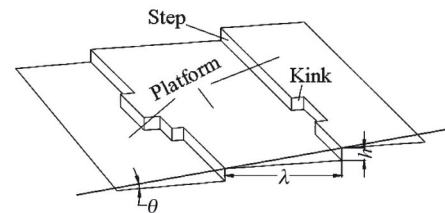

Fig.12   Schematic diagram of platform-step-kink model on free surface

and λ is the platform length.

The grain boundary energy depends on the misorientation between grains, and the equilibrium shape can be acquired by calculating the grain boundary energy. The grain boundaries decompose into stepped grain boundaries with several less closely packed planes. This decomposition can effectively reduce the energy of deformed grains. Andrejeva et al[17] observed the step-like grain boundaries in pure Nb during annealing, which were near to the CSL planes. Muschik et al[18] observed the facet grain boundary of Cu bicrystals during annealing and proposed that the faceting can reduce the total interface energy by 15%–20% by computer simulation.

The Ni-based alloys in this work have a face-centered cubic (fcc) structure, and their closely-packed plane is {111} plane with the lowest surface energy. If the angle between the grain boundary and the low-energy surface is small, the stepped grain boundary appears to ameliorate the deviation until the plane reaches a stable state. Gleiter et al[19] investigated the step-like grain boundaries in fcc metals by TEM. It is concluded that the interaction between {111} planes and the grain boundary can form a step structure in fcc materials. Therefore, the faceted structure can be found at both the

regular grain boundaries and the twin boundaries. According to Fig.8 and Fig.9, the steps have different angles and heights, indicating that the steps may be formed by different low-energy planes and different layers of low-energy planes. In crystallography, the angles between crystal planes of different forms are different. Therefore, the stepped grain boundaries formed by the decomposition of different low-energy interfaces differ in angle.

Based on TEM observations, it is confirmed that the faceting mainly occurs at the twin boundary around the low zone axis. The matrix of Ni-based alloys has fcc structure with low stacking fault energy, so it is easy to form annealing twins during the recrystallization. According to the growth accident mechanism and the special interface decomposition mechanism of the annealed twin boundary, the annealed twin boundary is usually linear in the form of straight-line pairs, steps, or bends. In this research, the annealing twins show the step shape, as shown in Fig.10a. The appearance of stepped twin boundary is considered as a typical faceting phenomenon, where the original grain boundaries break into flat segments with lower energy by faceting. Most cases occur near the coincidence sites and are affected by temperature and misorientation. Generally, the higher the temperature, the more the deviation from the coherent orientation, and the less the number of facets. Because of the high solution annealing temperature of nickel-based alloy, the number of stepped grain boundaries in the specimen is less. The facets in $\Sigma 3$ grain boundaries have a fixed morphology. Straumal et al[16] investigated the faceting of $\Sigma 3$ grain boundaries in copper at different temperatures, and observed several groups of typical facets relations. The facets of $\{111\}_1/\{111\}_2$ plane form an angle of 82° with 9R structure, and the facets of $\{111\}_1/\{111\}_2$ plane form an angle of 90° with $\{211\}_1/\{211\}_2$ plane. The $\{111\}_1/\{111\}_2$ facet or $\{112\}_1/\{112\}_2$ facet on $\Sigma 3$ grain boundary disappears or appears with changing the temperatures. The energy of $\{111\}_1/\{111\}_2$ plane is lower than that of $\{112\}_1/\{112\}_2$ plane. Both of them are stable at high temperatures, so the facet of $\Sigma 3$ grain boundary is mainly rectangular step composed of $\{111\}_1/\{111\}_2$ and $\{112\}_1/\{112\}_2$ facets.

Grain boundary migration is similar to the crystal surface growth in geometric structure. According to Fig.12, the vicinal surface is faceted, so it may contain steps and kink sites. The nucleation and propagation of the kink sites cause the growth of vicinal surface based on the step flow mechanism.

Generally, the grain boundaries are not atomically flat because they contain atomic steps and kinks. Foreign atoms are easily absorbed and emitted at the steps or kinks on the grain boundary, resulting in the grain boundary defects. Hadian et al[20] used molecular dynamics simulation to study the atomic migration mechanism of stepped grain boundaries and proposed the double-kink nucleation mechanism of stepped grain boundaries. The movement of stepped grain boundaries and the unstable flow of grains near the grain boundary jointly result in the grain growth, abatement, or rearrangement. Under this driving force, the atoms or atomic groups separate from the receding grains and move along the steps and across the grain boundaries with a certain thickness. Meanwhile, the growing grains absorb the same number of atoms to from the grain boundaries. Atom emission and absorption are the micro-mechanism of grain boundary migration, resulting in the fact that the step platform is a mostly closely-packed or less closely-packed plane. However, the step movement is affected by the pinning effect of inherent defects in the grain boundaries. The pinning slows down the movement of grain boundaries during the recrystallization. However, due to the pinning effect, several atomic platforms of steps are pinned and merged by other moving steps, thus forming the micrometer-scale steps, as shown in Fig. 8 and Fig. 9. Rajabzadeh et al[21] investigated the lateral motion of grain boundaries in the bi-crystalline and polycrystalline Al. It is revealed that the moving step can interact with the lattice dislocations and become immobile. The immobile step can be merged by the subsequent steps and the accumulation of grain boundary dislocation steps finally leads to the macro-steps. Bowers et al[22] investigated the structural fluctuations at the incommensurate grain boundary in Au. It is reported that the lateral motion of grain boundaries by collective motion involves the constriction and expansion of stacking fault and steps. In actual recrystallization, the rapid migration of the grain boundary is caused by the continuous nucleation and propagation of steps composed of grain boundary dislocation.

The driving force of grain boundary migration is the distortion energy between the recrystallization region and the deformation region in the recrystallization. The migration of annealing twins has its own kinetics. The $\{111\}_1/\{111\}_2$ CSL plane is dislocation-free and has low grain boundary energy, so it is approximately stable during the recrystallization procedure. However, the $\{112\}_1/\{112\}_2$ CSL plane has a large number of dislocations, which are beneficial to migration. Xu et al[23] investigated the migration of (111) twin boundary with $(11\bar{2})$ steps in nanocrystal copper and found that the (111) twin boundary migrates along the $(11\bar{2})$ step direction rather than the direction perpendicular to the normal direction of (111) plane. The migration of $\{112\}$ twin plane involves the atom motion in the whole interface, so it may be a thermal activated process rather than a simple dislocation slip. Firstly, the migration of $\{112\}$ twin boundary needs the nucleation at the $\{111\}$ grain boundary corner, which subsequently promotes the migration of the whole grain boundary. This is similar to the movement of the edge dislocation with a large Burger's vector, as shown in Fig. 13. The reduction of the $\{111\}$ twin plane is the driving force of the migration of $\{112\}$ twin boundary. Xu et al[23] reported that this driving force is much larger than that for the grain growth with general grain boundaries. As a result, partial elimination of $\{111\}$ twin plane can accelerate the grain boundary migration. If the driving force of recrystallization process is sufficiently large, the migration of $\{112\}$ twin boundary can generate additional $\{111\}$ twin plane, resulting in the twin grain growth. Therefore, the progressive migration of $\{112\}$ twin boundary results in the enlargement or shrinkage of twins.

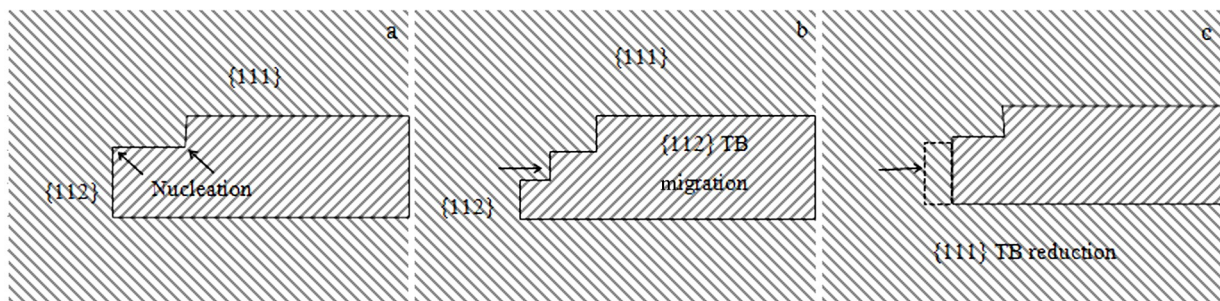Fig. 14 shows TEM morphologies of GH4760 alloys after

Fig.13 Schematic diagrams of migration of stepped twin boundary: (a) nucleation at step corner; (b) {112} twin boundary migration; (c) reduced {111} twin boundary after migration (TB: twin boundary)
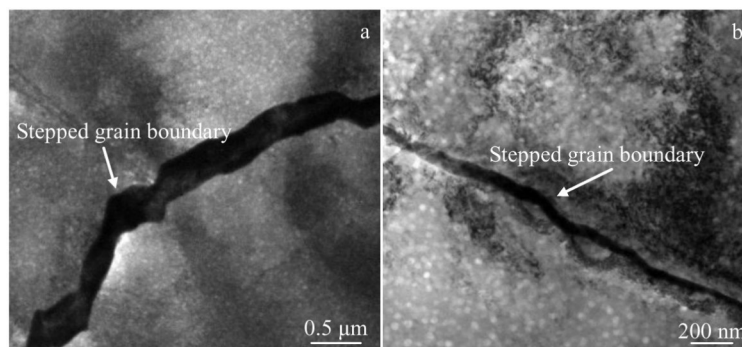

Fig.14 TEM morphologies of stepped grain boundaries of GH4760 alloys after different solution and aging treatments: (a) 1160 °C/20 min/water cooling+800 °C/16 h/air cooling; (b) 1160 °C/40 min/water cooling+800 °C/16 h/air cooling

standard solution and aging treatment. After recrystallization, the stepped grain boundaries still exist, which indicates that the stepped grain boundaries partially remain after recrystallization, thus affecting the material properties.

3 Conclusions

1) In the hot deformation processes of GH4760, GH4738, and AD730 Ni-based alloys, the dynamic recrystallization is dominated by the discontinuous nucleation mechanism via the bowing of grain boundaries. Static recrystallization during the solution treatment of cold-rolled GH4760 alloy and as-forged GH4738 alloy is dominated by the strain-induced grain boundary migration mechanism.

2) Different forms of stepped grain boundaries are produced during dynamic and static recrystallizations in order to form the low-index planes with low energy, thereby reducing the grain boundary interface energy. The stepped grain boundaries at the Σ3 grain boundaries have fixed morphology. Most grain boundaries decompose into the $\{111\}_1/\{111\}_2$ and 90° $\{112\}_1/\{112\}_2$ facets. The stepped grain boundary migrates rapidly, which promotes the grain boundary migration and accelerates the recrystallization. Partial stepped grain boundaries remain after the recrystallization, thus affecting the material properties.

References

1 Chang K M, Liu X B. *Materials Science and Engineering A*[J], 2001, 308(1–2): 1

2 Masoumi F, Jahazi M, Shahriari D *et al. Journal of Alloys and Compounds*[J], 2016, 658: 981

3 Guo Jianting. *Materials Science and Engineering for Superalloys* [M]. Beijing: Science Press, 2008: 3 (in Chinese)

4 Wang L, Wang S A, Liu Y *et al. Material Science Forum*[J], 2010, 638: 2357

5 Liu Y X, Lin Y C, Li H B *et al. Materials Science and Engineering A*[J], 2015, 626: 432

6 Lee S B, Yoon D K, Hwang N M *et al. Metallurgical and Materials Transactions A*[J], 2000, 31(3): 985

7 Kim K J, Hong H U, Nam S W. *Materials Chemistry and Physics* [J], 2011, 126(3): 480

8 Hong H U, Jeong H W, Kim I S *et al. Philosophical Magazine* [J], 2012, 92(22): 2809

9 Jiang L, Hu R, Kou H C *et al. Materials Science and Engineering A*[J], 2012, 536: 37

10 Yao Zhihao, Dong Jianxin, Zhang Maicang *et al. Rare Metal Materials and Engineering*[J], 2017, 46(11): 3382 (in Chinese)

11 Li D F, Guo Q M, Guo S L *et al. Materials & Design*[J], 2011, 32(2): 696

12 Cao Y, Di H S, Zhang J Q *et al. Materials Science and Engineering A*[J], 2013, 585: 71

13 Humphreys F J, Hatherly M. *Recrystallization and Related Annealing Phenomena*[M]. Amsterdam: Elsevier, 2004: 169

14 Straumal B B, Polyakov S A, Bischoff E *et al. Interface Science*[J], 2001, 9(3–4): 287

15 Straumal B B, Semenov V N, Khruzhcheva A S *et al. Journal of Materials Science*[J], 2005, 40(4): 871

16 Straumal B B, Polyakov S A, Mittemeijer E J. *Acta Materialia*[J], 2006, 54(1): 167

17 Andrejeva A V, Salnikov G I, Fionova L K. *Acta Metallurgica*[J], 1978, 26(9): 1331

18 Muschik T, Laub W, Wolf U *et al. Acta Metallurgica et Materialia*[J], 1993, 41(7): 2163

19 Gleiter H. *Acta Metallurgica*[J], 1969, 175(5): 565

20 Hadian R, Grabowski B, Race P C *et al. Physical Review B*[J], 2016, 94: 165 413

21 Rajabzadeh A, Legros M, Combe N *et al. Philosophical Magazine*[J], 2013, 93(10–12): 1299

22 Bowers M L, Ophus C, Gautam A *et al. Physical Review Letters*[J], 2016, 116: 106 102

23 Xu L H, Xu D, Tu K N *et al. Journal of Applied Physics*[J], 2008, 104(11): 113 717

典型镍基高温合金的再结晶机理

史宸伊，张麦仓，郭　晶

(北京科技大学 材料科学与工程学院，北京 100083)

摘　要： 研究了GH4760、GH4738和AD730典型镍基高温合金在热变形过程中的动态和静态再结晶行为，并进行了压缩热变形和固溶退火实验。结果表明，动态和静态再结晶的成核机制以涉及晶界凸起的不连续机理为主。在动态和静态再结晶过程中，普通晶面向低指数晶面转变，产生了不同类型的台阶晶界，这种转变将使更多的晶面具有较低的能量。$\Sigma3$晶界上阶梯边界的形貌大多分解为$\{111\}_1/\{111\}_2$和$90°\{112\}_1/\{112\}_2$小平面。台阶状晶界促进了晶界迁移，加速了再结晶过程。再结晶完成后，部分台阶晶界保留，界面能降低，促进了后续晶粒生长。

关键词： 镍基高温合金；台阶状晶界；再结晶成核机制

作者简介：史宸伊，男，1998年生，硕士，北京科技大学材料科学与工程学院，北京 100083，电话：010-62332884，E-mail：s20200348@xs.ustb.edu.cn